Electronic Supplementary Material (ESI) for Journal of Materials Chemistry B
This journal is © The Royal Society of Chemistry 2014

Striped, bioactive Ce-TiO_2 material with peroxynitrite-scavenging activity

*A. Noel Gravina[a], Juan M. Ruso[b], Noelia L. D'Elia[a] , Juan A. Laiuppa[c], Graciela E. Santillán[c], Jose L. Marco-Brown[d], Paula V. Messina [a]**

(a) Department of Chemistry, Universidad Nacional del Sur, 8000, Bahía Blanca, Argentina. INQUISUR-CONICET (b) Soft Matter and Molecular Biophysics Group, Department of Applied Physics, University of Santiago de Compostela, Santiago de Compostela, 15782, Spain. (c) Department of Biology, Biochemistry and Pharmacy, Universidad Nacional del Sur, (8000) Bahía Blanca, Argentina (d) Department of Inorganic Chemistry, Analytics and Physical Chemistry, INQUIMAE, FCEN, Universidad de Buenos Aires, Pabellón II, C1428EHA, Buenos Aires, Argentina.

* Author to whom correspondence should be addressed. Tel: +54 291 4595159. Fax: +54 291 4595160. Electronic mail: pmessina@uns.edu.ar.

Structural characterization: microcrystalline and topographical analysis.

All samples were constituted for small prismatic nano-particles of about 30-50 nm length, and Ce-atoms presence during material synthesis decreased the particle size.

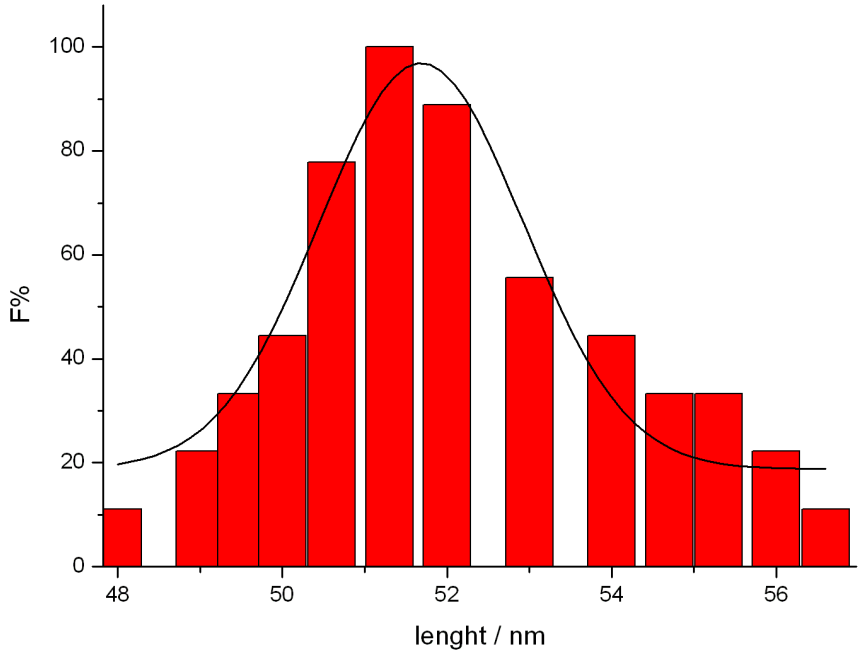

Figure ESI1: Size distribution histograms of MI nano-particles.

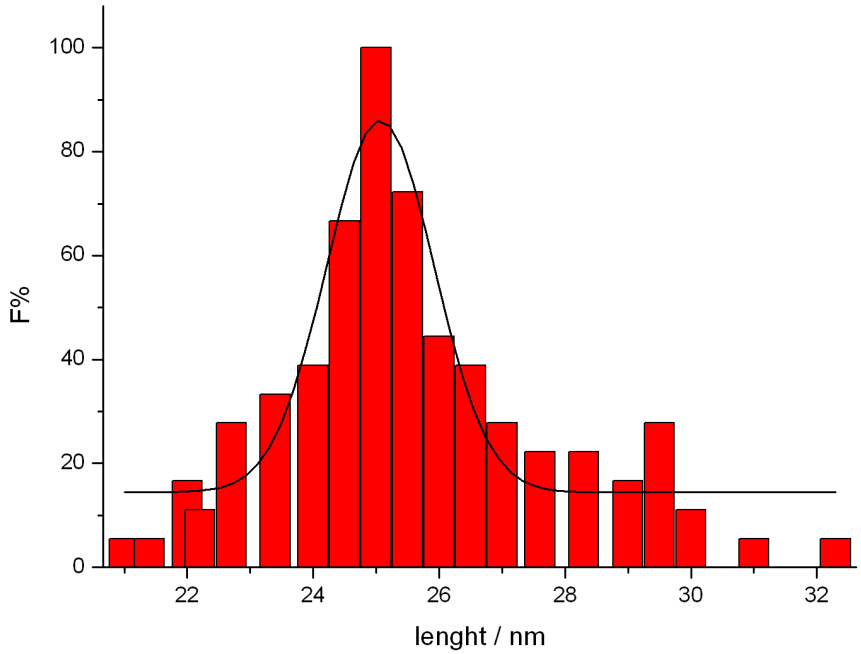

Figure ESI2: Size distribution histograms of MII nano-particles.

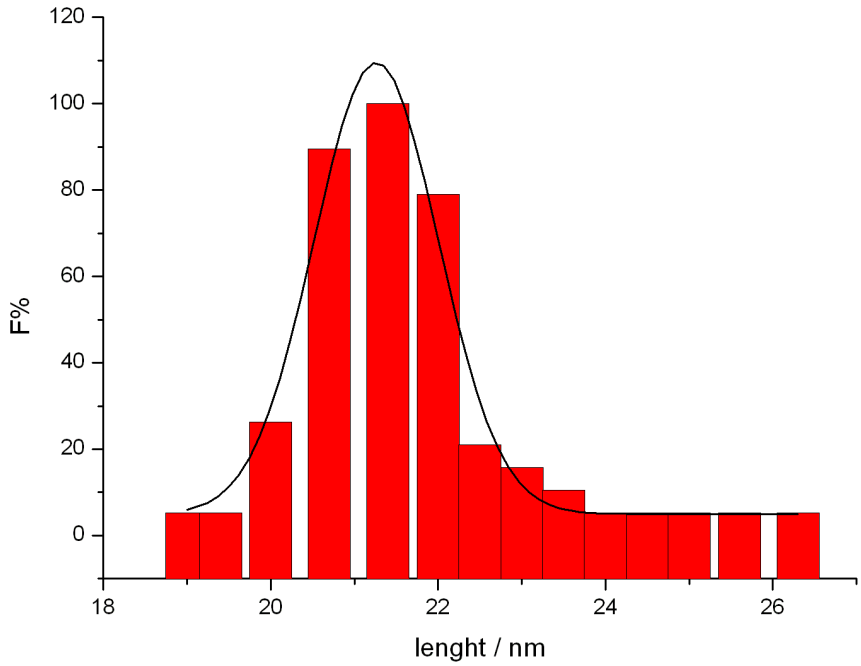

Figure ESI3: Size distribution histograms of MIII nano-particles.

The diffraction patterns clearly indicates that all samples before annealing are constituted for a pure anatase phase (tetragonal, I41/amd, JCPDS cards 21-1272).

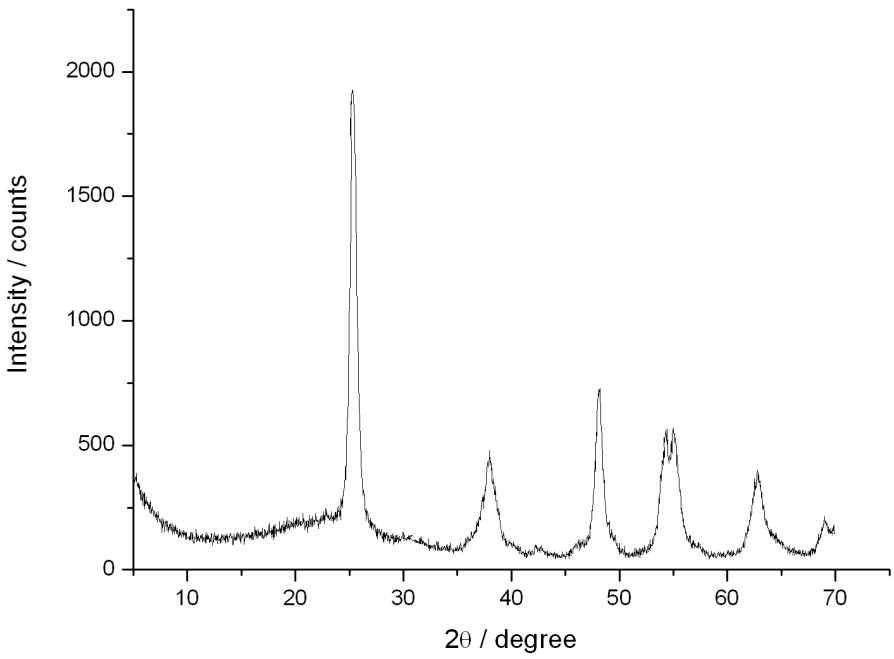

Figure ESI4: X-Ray diffraction pattern of MI material before annealing

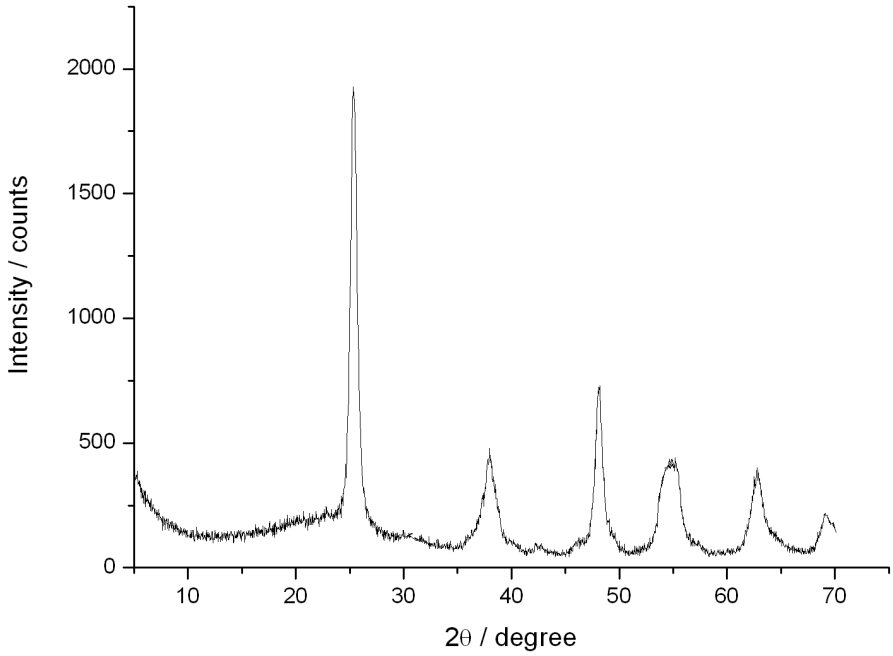

Figure ESI5: X-Ray diffraction pattern of MII material before annealing

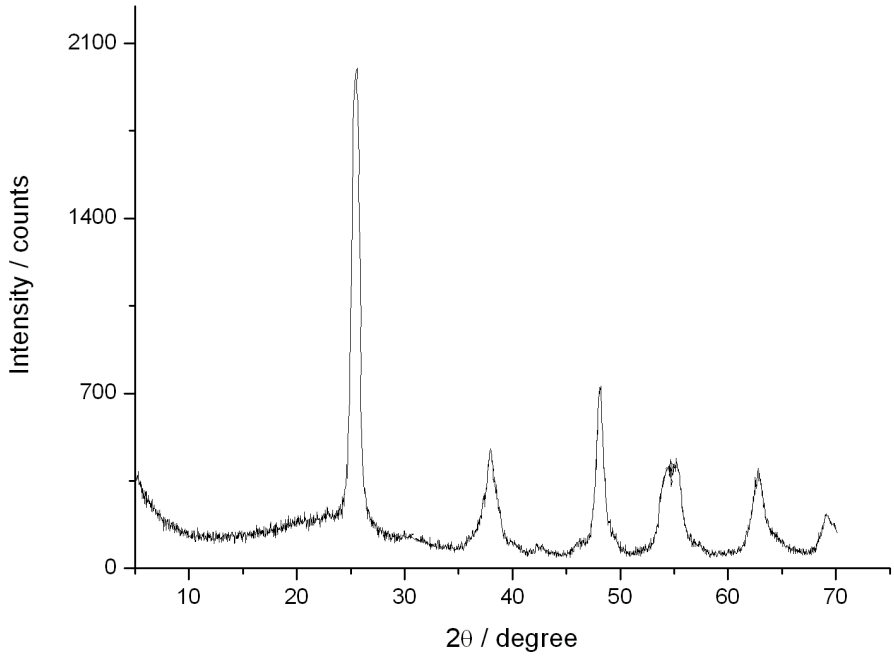

Figure ESI6: X-Ray diffraction pattern of MIII material before annealing

After calcination at 650ºC, MI is partially transformed in TiO_2 rutile in accordance with anatase to rutile transition that occurs at 600ºC and 1 atm [1], while MII and MIII continued being anatase.

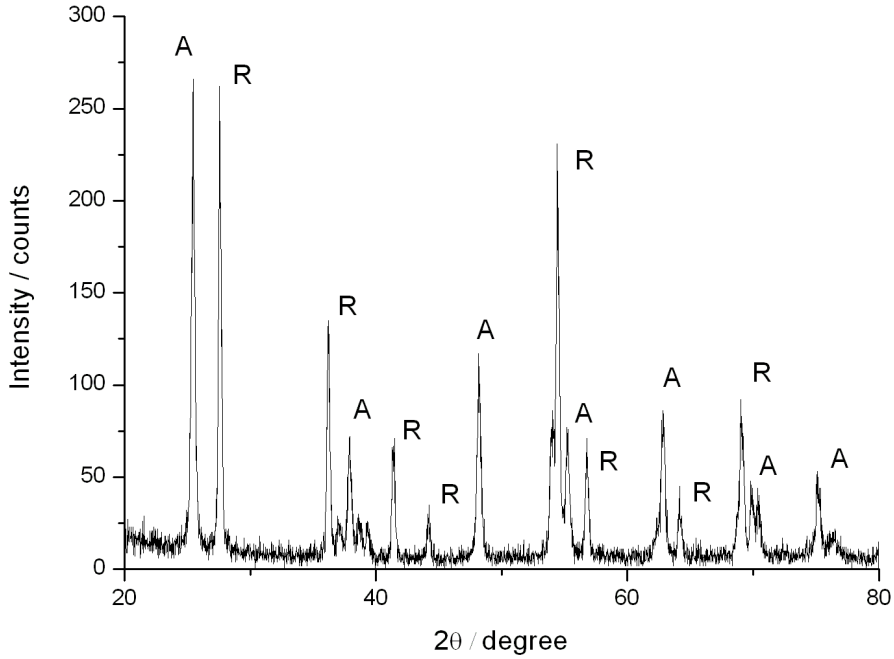

Figure ESI7: X-Ray diffraction pattern of MI material after annealing. (A) anatase, (R) rutile.

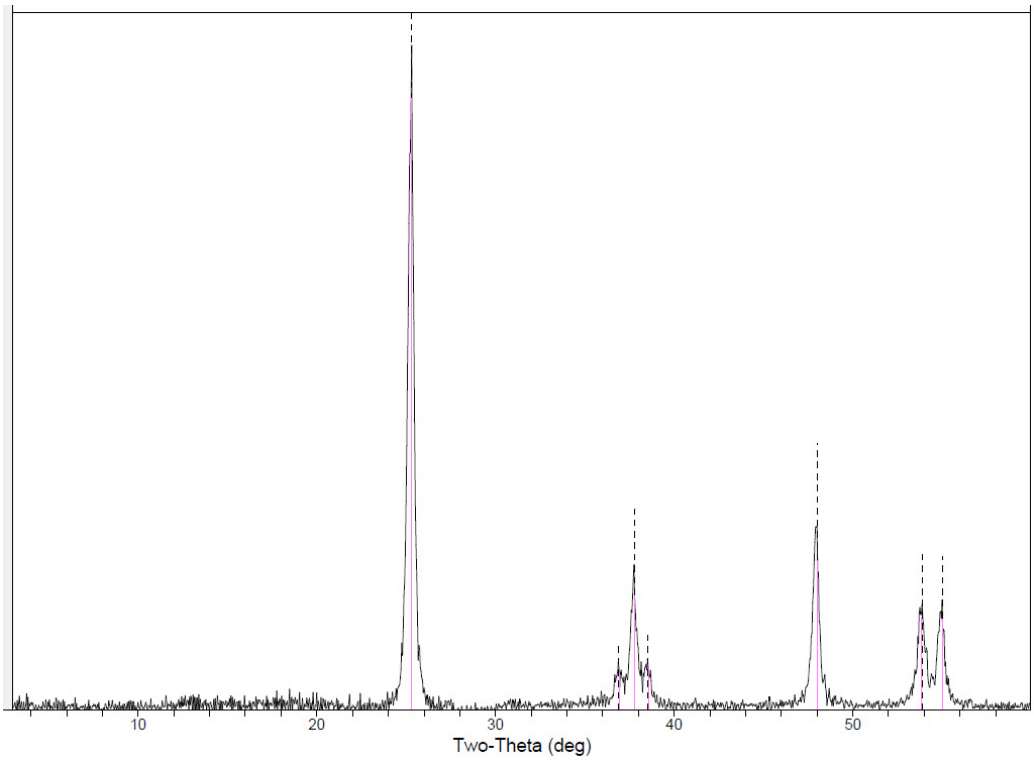

Figure ESI8: X-Ray diffraction pattern of MII material after annealing

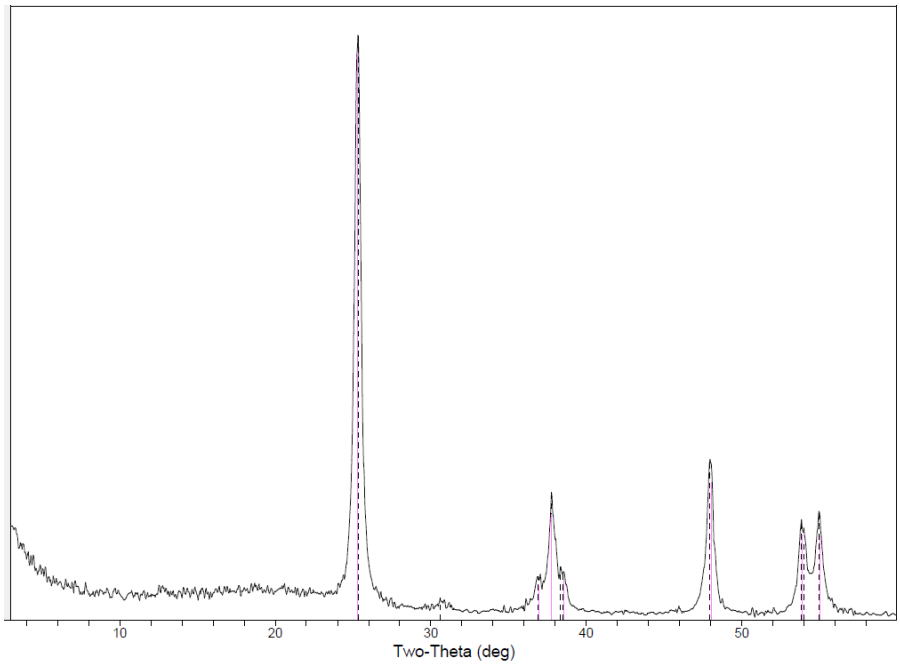

Figure ESI9: X-Ray diffraction pattern of MIII material after annealing.

The absence of diffraction peaks at 31º shows that the samples always were free from TiO_2 brookite structures. No trace of diffraction peaks due to cerium oxide was detected from X-ray diffraction patters or from X-ray energy dispersive (EDX) microanalysis. This is attributed to the small amount and the high area of distribution of the dopant around titania particles. The incorporation of Ce atoms to anatase lattice was denoted for the variation of "*a*" and "*c*" lattice parameter, **table 1** in the manuscript.

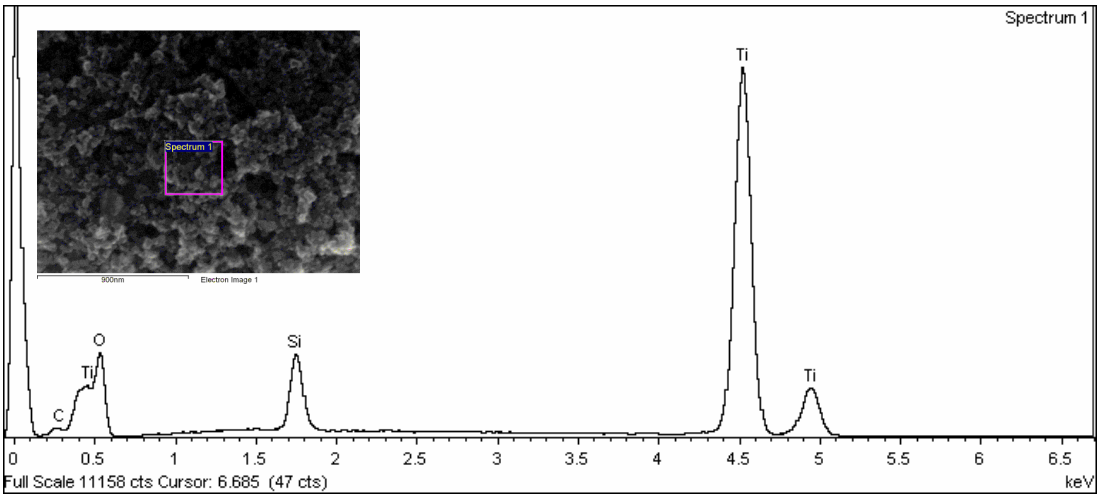

Figure ESI10: EDX patters of MI material after annealing.

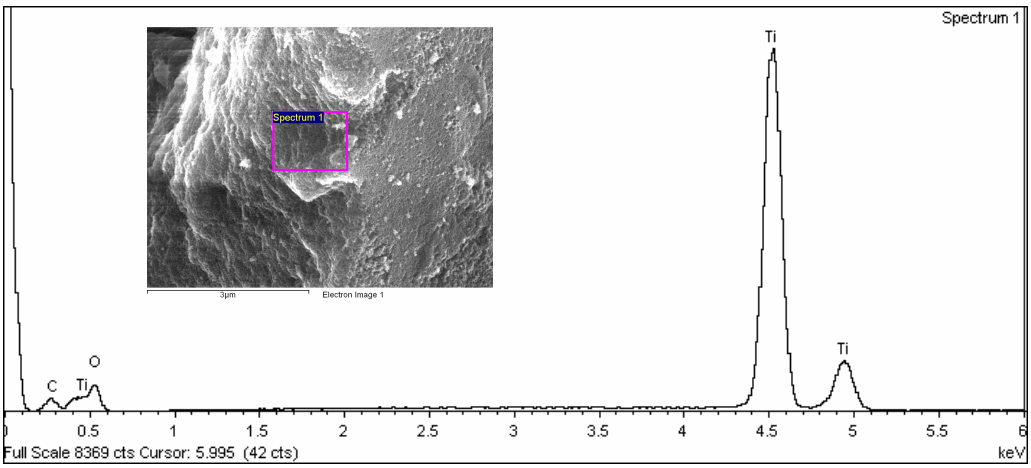

Figure ESI11: EDX patters of MII material after annealing.

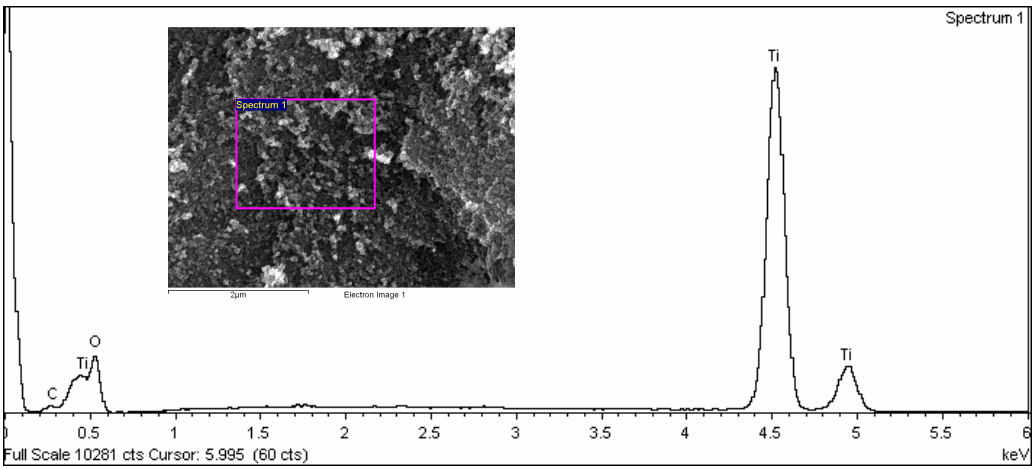

Figure ESI12: EDX patters of MIII material after annealing

Description of Rugosity Parameters

The arithmetic average height parameter (R_a), also known as the centre line average (CLA), is the most universally used roughness parameter for general quality control. It is defined as the average absolute deviation of the roughness irregularities from the mean line over sampling length. The mathematical definition and the digital implementation of the arithmetic average height parameter are, respectively, as follows[2].

$$R_a = \frac{1}{n}\int_0^l |y(x)|dx \qquad (1)$$

$$R_a = \frac{1}{n}\sum_{i=1}^{n}|y_i| \tag{2}$$

To represent the standard deviation of the surface height distribution, the root mean square roughness (R_q) was used. It is an important parameter to describe the surface roughness by statistical method. This parameter is more sensible than the arithmetic average height (R_a) to large deviation from the mean line. The mathematical definition and the digital implementation are as follows[2]:

$$R_q = \sqrt{\frac{1}{l}\int_0^l \{y(x)\}^2 dx} \tag{3}$$

$$R_q = \sqrt{\frac{1}{n}\sum_{i=1}^{n} y_i^{\,2}} \tag{4}$$

The R_q mean line is the line that divides the profile so that the sum of the squares of the deviations of the profile height from it is equal to zero.

Maximum height of peaks (R_p) and maximum deep of valleys (R_v) are defined as the maximum height and the maximum depth of the profile above and below the mean line within the assessment of the length. The relationship between them is defined as the maximum height of the profile (R_t)

$$R_p = \max_i y_i \tag{5}$$

$$R_v = \min_i y_i \tag{6}$$

$$R_t = R_p - R_v \tag{7}$$

To measure the symmetry of the roughness profile about the mean line, the profile skewness was analyzed. This parameter is sensitive to occasional deep valleys or high peaks. A symmetrical height distribution, i.e. with identical peaks and valleys, has zero skewness. Profile with peaks removed or deep scratches have negative skewness. Profiles with valleys filled in or high peaks have positive skewness. Skewness parameter (R_{sk}) can be used to distinguish between two profiles having the same R_a or R_q values but with different shapes. The mathematical and the numerical formula used to calculate the skewness of a profile, which has a number N of points, are as follows:

$$R_{sk} = \frac{1}{R_q^{\,3}}\int_{-\infty}^{\infty} y^3 p(y) dy \tag{8}$$

$$R_{sk} = \frac{1}{NR_q^{\,3}}\left(\sum_{i=1}^{N} Y_i^{\,3}\right) \tag{9}$$

where Y_i is the height of the profile at point number i.

Kurtosis coefficient (R_{ku}) describes the sharpness of the profile probability density. If $R_{ku} < 3$ the distribution curve is said to be platykurtoic and has relatively few high peaks and low valleys. If $R_{ku} > 3$ the distribution curve is said to be leptokurtoic and has relatively many high peaks and low valleys. The kurtosis parameter can also be used to differentiate between surfaces, which have different shapes and the same value of R_a.

$$R_{ku} = \frac{1}{R_q^{\,4}}\int_{-\infty}^{\infty} y^4 p(y)dy \tag{10}$$

$$R_{ku} = \frac{1}{NR_q^{\,4}}\left(\sum_{i=1}^{N} Y_i^{\,4}\right) \tag{11}$$

The fractal architecture should also be assessed, since this concept is particularly interesting in surfaces and material science. Natural fractals are repetitive patterns that self-similar across a finite range of scales and many biological structures, including bone, are fractal or even fractal-like. Its influence and relevance on biological tissue is unknown, but implant surfaces might reveal this type of repetitive patterns at the micro-, nano- and crystal scales during quantitative morphology. To compute fractal dimension (D_f), the box counting method was applied to different SEM images. This protocol was used in a previous work [3] and consists of applying an increasingly fine grid over the area studied and counting, at each iteration, the number of boxes containing at least one part of the object to be measured. The fractal dimension *Df* is then linked to the number *n(s)* of boxes of dimension *s* necessary to fill the surface area of the particle according to[4]:

$$D_f = \lim_{s\to 0}\frac{\ln n(s)}{\ln(1/s)} \tag{12}$$

This method was also optimized by means of a calculation procedure stemming from the work of Foroutan-Pour *et al.*[5] which allows a precise determination of key parameters of the method, namely the number and the dimensions of the boxes[6]. The images, initially with 256 grey levels and 1024 × 768 pixels in size, are converted to binary images. The fractal dimension is then derived from the slope of a least-square linear fit of the plot of *log n* versus *log (box size)*, where *n* is the number of non-overlapping equal boxes that would

fill the projected surface area of the aggregate. This operation can be carried out by different software packages[7], Log–log representations of the calculations of fractal dimension on the systems studied are shown in **ESI13**.

Most authors, based on Minkowski–Bouligand dimension and the content of projections on the directions of the planes, have demonstrated that, in general, there is no general relationship between 3D and 2D fractal dimensions[8]. However, functional relationships between 2D and 3D fractal dimensions were found for specific systems, such as aluminum oxide nanoparticles,[9]assuming a uniform mass distribution of the object along the third dimension:

$$D_{3D} = 0.47 D_{2D} + 1.78 \quad (13)$$

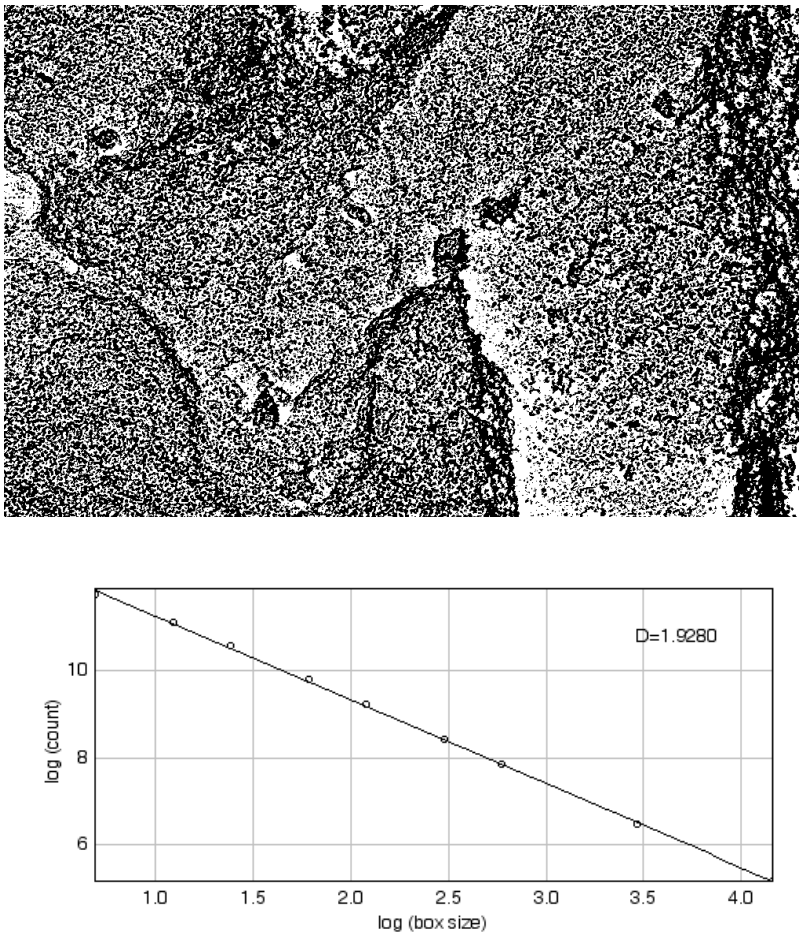

Figure ESI13: Example of fractal dimension calculus from the binary 8bits SEM image of the MIII material after annealing.

Bioactivity assay

EDX microanalysis indicated that the Ca/P ≈ 1.60 which could be ascribed to stoichiometric HA.

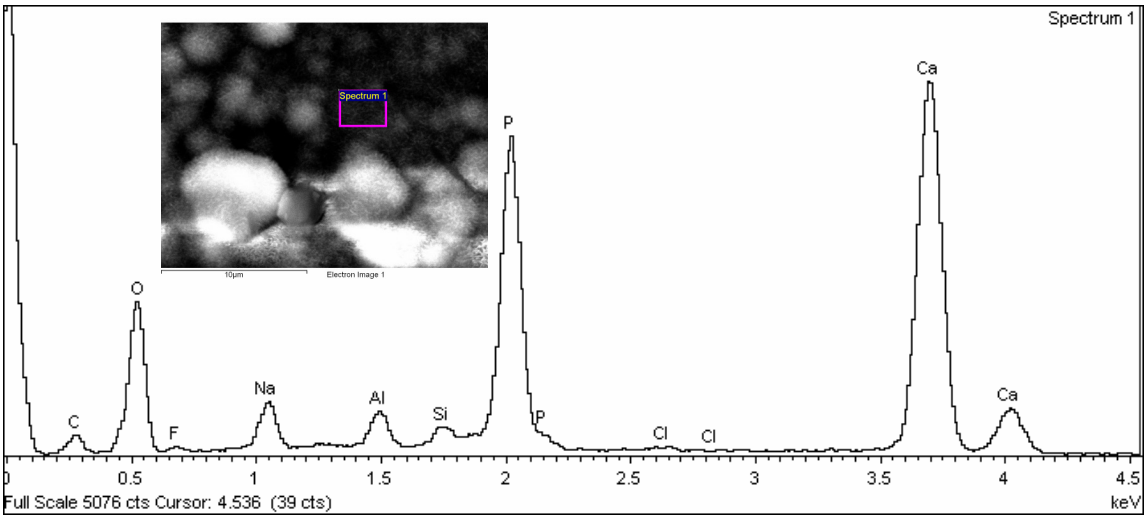

Figure ESI14: EDX microanalysis of HA layer developed on MII after 10 day of immersion in 1.5 SBF at 37ºC.

Giemsa stain of neonatal calvarian osteoblast after 72h of treatment in the presence of TiO_2 and TiO_2- CeO_2 materials exclude any negative effect of the material crystalline microstucture, morphology and CeO_2 presence in the cells survival and in their morphology.

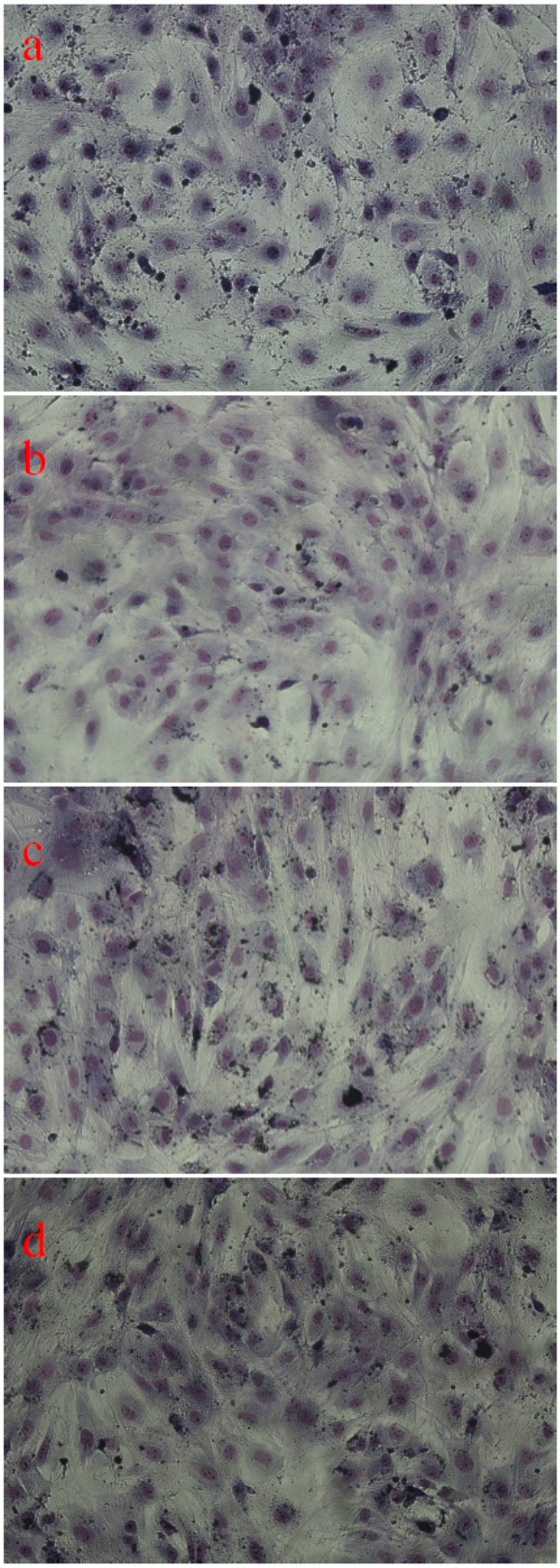
a
b
c
d

Figure ESI15: Microphotographs of Giemsa stained osteoblasts after 72h of treatment. (a) control, (b) in the presence of material containing [CeO_2] = 0.05 wt%, (c) in the presence of material containing [CeO_2] = 0.08 wt%, (d) in the presence of material containing [CeO_2] = 0.10 wt%.

Isothermal Peroxynitrite ($ONOO^-$) decay

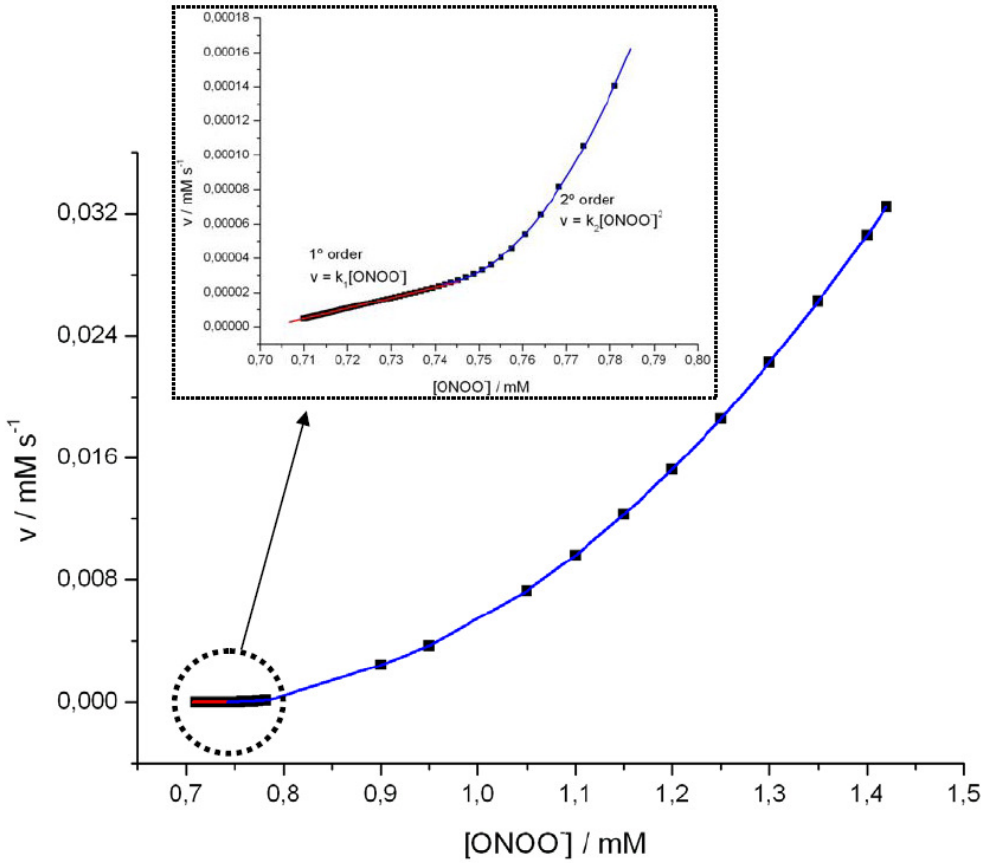

Figure ESI16: $ONOO^-$ degradation velocity in presence of MII material as a function of [$ONOO^-$]. T= 25ºC, pH = 13.1

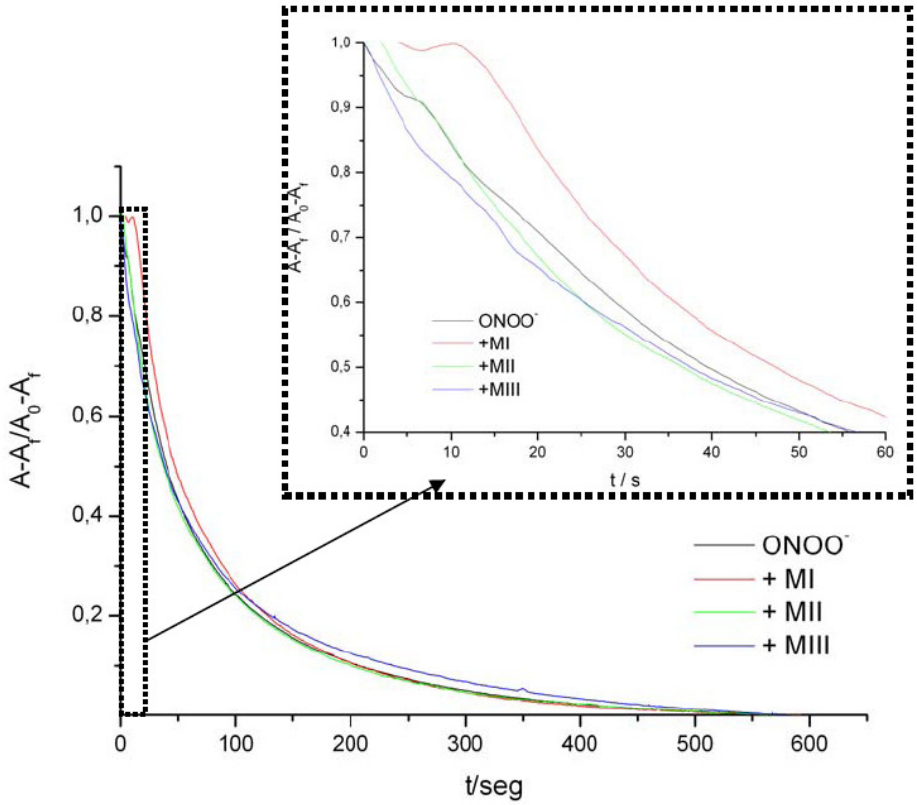

Figure ESI17: ONOO$^-$ degradation in presence and absence of material in PBS solution at 25ºC.

References.

(1) Dachile, F.; Simons, P. Y.; Roy, R. *The American mineralogist.* **1968**, *53*, 1929.

(2) Gadelmawla, E. S.; Koura, M. M.; Maksoud, T. M. A.; Elewa, I. M.; Soliman, H. H. *Journal of Materials Processing Technology* **2002**, *123*, 133.

(3) Hassan, N.; Soltero, A.; Pozzo, D.; Messina, P. V.; Ruso, J. M. *Soft Matter* **2012**, *8*, 9553.

(4) Giorgilli, A.; Casati, D.; Sironi, L.; Galgani, L. *Physics Letters A* **1986**, *115*, 202.

(5) Foroutan-pour, K.; Dutilleul, P.; Smith, D. L. *Applied Mathematics and Computation* **1999**, *105*, 195.

(6) Bau, S.; Witschger, O.; Gensdarmes, F.; Rastoix, O.; Thomas, D. *Powder Technology* **2010**, *200*, 190.

(7) Ibaseta, N.; Biscans, B. *Powder Technology* **2010**, *203*, 206.

(8) Akkari, H.; Bhouri, I.; Dubois, P.; Bedoui, M. H. *Mathematical Modelling of Natural Phenomena* **2008**, *3*, 48.

Electronic Supplementary Material (ESI) for Journal of Materials Chemistry B
This journal is © The Royal Society of Chemistry 2014

(9) Ganguly, S.; Basu, S.; Sikdar, S. *Proceedings of the Institution of Mechanical Engineers, Part N: Journal of Nanoengineering and Nanosystems* **2012**, *226*, 3.